A Multiwatt All Gas-Phase Iodine Laser (AGIL)

Gerald C. Manke, II, Chris B. Cooper, Shiv C. Dass, Timothy J. Madden, and Gordon D. Hager

***Abstract*—The demonstration and characterization of a multiwatt all gas-phase iodine laser (AGIL) are described. A 20-cm subsonic reactor was used to produce NCl($a^1\Delta$) for a series parametric studies of the $I^*(^2P_{1/2}) - I(^2P_{3/2})$ small-signal gain and extracted power dependence on reactant flow rates and reaction time. The highest measured gain was 2.5×10^{-4} cm^{-1} and the highest power observed was 15 W.**

***Index Terms*—All gas iodine laser (AGIL), chemical lasers, chemical oxygen iodine laser (COIL).**

I. Introduction

SINCE the invention of the chemical oxygen iodine laser (COIL) in the mid-1970s [1], there has been interest in energy carrier molecules that react via energy transfer with ground state iodine atoms to generate an inversion on the electronic spin-orbit transition. Singlet delta oxygen, for example, efficiently generates $I^*(^2P_{1/2})$ via

$$O_2(a^1\Delta) + I \rightarrow O_2(X^3\Sigma^-) + I^*(^2P_{1/2}). \quad (1)$$

In principle, all molecules with the $(p\pi^*)^2(p\sigma^*)^0$ electronic configuration will have the same electronic states as O_2, i.e., $(X^3\Sigma^-)$, $(a^1\Delta)$, and $(b^1\Sigma^+)$. Because of the selection rules for electronic transitions, the singlet delta state is metastable. The singlet nitrenes in particular (i.e., NF and NCl) have been investigated as possible replacements or alternatives to $O_2(a^1\Delta)$ because they share the requisite $(p\pi^*)^2(p\sigma^*)^0$ electronic configuration [2]. These metastable molecules have radiative lifetimes in the 2–5 s range [3]–[5] and have the potential to be useful energy carriers in energy transfer chemical laser applications.

Unfortunately, metastability is not the only figure of merit for chemical laser devices based on an energy transfer process. The ability to transfer energy to a suitable laser species (such as iodine atoms) depends on the detailed kinetics and dynamics of the interaction between the energy donor and acceptor, which are determined by the details of the complex multidimensional potential energy surfaces that govern the interaction [2].

To date, only NF($a^1\Delta$) and NCl($a^1\Delta$) have been found to have the properties necessary to serve as energy carriers. Namely, both have long radiative lifetimes and are relatively inert to chemical reaction and physical quenching [6], [7]. Indeed, there have been several demonstrations of efficient energy transfer from NF($a^1\Delta$) to Bi [8], [9], BiF [10]–[12], and BH [13]–[15]. Unfortunately, these systems were not suitable for generating high-energy chemical lasers [2]. Attempts to generate an NF($a^1\Delta$)/I energy transfer laser have also failed [16]. The reason for this failure is that despite the fast reaction of NF($a^1\Delta$) with atomic iodine ($k_2 = 1.8 \pm 0.4 \times 10^{-11}$ cm^{3}molecule^{-1}s^{-1}) [17]

$$NF(a^1\Delta) + I \rightarrow NF(X^3\Sigma^-) + I^* \quad (2a)$$

$$\rightarrow \text{products} \quad (2b)$$

an inversion is prevented by a poor branching fraction for (2a) (~10%–20%) and fast quenching of I^* by NF($a^1\Delta$) ($k_3 = 5.7 \times 10^{-11}$ cm^{3}molecules^{-1}s^{-1}) [17], [18]

$$NF(a^1\Delta) + I^* \rightarrow NF(b^1\Sigma^+) + I(^2P_{3/2}). \quad (3)$$

On the other hand, NCl($a^1\Delta$) not only has a fast reaction with atomic iodine ($k_4 = 1.5 \pm 0.7 \times 10^{-11}$ cm^{3}molecules^{-1}s^{-1}) [19], [20]

$$NCl(a^1\Delta) + I \rightarrow NCl(X^3\Sigma^-) + I^* \quad (4a)$$

$$\rightarrow \text{products} \quad (4b)$$

but the branching fraction for the $I^*(^2P_{3/2})$ formation is large ($\Gamma \geq 0.7$) [20] and the energy-pooling reaction between NCl($a^1\Delta$) and $I^*(^2P_{1/2})$ does not appear to be important. Hence, NCl($a^1\Delta$) should be an efficient energy carrier suitable for a scalable energy transfer chemical iodine laser.

Indeed, a subsonic continuous-wave chemical $I^*(^2P_{1/2})$ laser pumped by NCl($a^1\Delta$) was reported by Henshaw and co-workers in 2000 [21]. In their experiment, the energy carrier NCl($a^1\Delta$) was produced from F atoms and hydrogen azide by a three-step process [20], [22]–[24]

$$F + DCl \rightarrow DF + Cl \quad (5)$$

$$Cl + HN_3 \rightarrow HCl + N_3 \quad (6)$$

$$Cl + N_3 \rightarrow NCl(a^1\Delta) + N_2. \quad (7)$$

The authors named their discovery the all gas-phase iodine laser (AGIL). Their demonstration was motivated and enabled by the small-signal gain measurements of Herbelin, *et al.* [25], Bower *et al.* [26], and the transient lasing demonstration of Ray and Coombe [27]. Other milestones in the history of AGIL are discussed in detail elsewhere [2].

Since the initial subwatt laser demonstration [21], there has been considerable effort expended to scale this device to multiwatt powers. This paper summarizes the results of these experiments.

II. Experimental Methods

A new subsonic flow device for the generation of NCl($a^1\Delta$) was constructed following the completion of the work that cul-

Manuscript received October 31, 2002; revised April 1, 2003. This work was supported by the Air Force Office of Scientific Research (AFOSR).

G. C. Manke, II, T. J. Madden, and G. D. Hager are with the Air Force Research Laboratory, Directed Energy Directorate, Kirtland AFB, NM 87117 USA.

C. B. Cooper and S. C. Dass are with Boeing-Rocketdyne, Kirtland AFB, NM 87117 USA.

Digital Object Identifier 10.1109/JQE.2003.814381

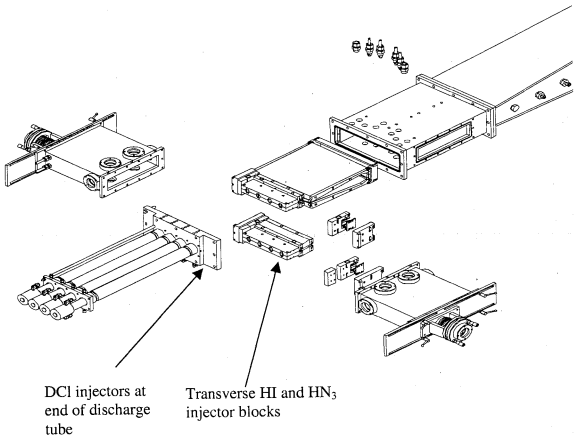

Fig. 1. Construction schematic for AGIL 2. Major components include the four discharge tubes with radial He and DCl injectors attached to the ends, HI and HN_3 injector blocks, flow reactor with adjustable ramps, He injectors for containment of the flow, and laser mirror tunnels and mounts.

minated in the demonstration of a 180-mW AGIL device. The new reactor (AGIL 2) is very similar in design to the old device (AGIL 1) [21], [25], [28] in terms of materials, geometry, and injector locations. The most significant changes are the optical path length was increased to 20 cm (as opposed to 5 cm), F atoms are produced by four discharge tubes (as opposed to one), and the purge flows along the sides of the reactor were improved to provide better containment of the reactive flow. A construction schematic of AGIL 2 is shown in Fig. 1. The flow-channel height in the injector block section and the separation between the HI and HN_3 injectors are adjustable. To accommodate heat release, area relief is provided by an adjustable ramp. The experiments described here reproduce the AGIL 1 device geometry.

The four discharge tubes are powered by a power supply and cooled by chilled water. Fluorine atoms are generated when either pure NF_3 or a mixture of 20% F_2 in He are diluted with 6 mmol s^{-1} of He and passed through the discharges. The power supply was powerful enough to dissociate 1 mmol s^{-1} of F_2 or 1.5 mmol s^{-1} of NF_3 such that approximately 2 mmol s^{-1} of F atoms were generated. Higher flow rates of F_2 (20% in He) led to incomplete dissociation, while higher flow rates of NF_3 extinguished the discharge. NF_3 is the preferred F atom source because it does not produce any molecular fluorine which would react with Cl and I to generate IF and ClF—strong quenchers of $I^*(^2P_{1/2})$ and $NCl(a^1\Delta)$. The new power supply was routinely operated at maximum current per tube which allowed higher F_2 and NF_3 flow rates and yielded larger F atom flows than previously generated in AGIL 1 [28].

Helium and deuterium chloride are added through radial injectors at the end of each discharge tube to convert the flow of F atoms into Cl atoms (The He flow rate was fixed at approximately 40 mmol s^{-1}). Hydrogen iodide was highly diluted to approximately 0.5% by adding $\sim$ 90 mmol s^{-1} of He prior to its injection into the reactor. Hydrogen azide was synthesized and stored in six 150 L tanks as a 10% mixture in He. Both HN_3 and HI were injected from the top and bottom walls into the flow downstream of the DCl injector. The HI and HN_3 injector blocks consisted of two rows of holes each.

TABLE I
TYPICAL EXPERIMENTAL CONDITIONS

Species	Flow Rates (mmol s^{-1}) AGIL 1 (Herbelin)[25]	AGIL 1 (Henshaw)[21]	AGIL 2 (this work)
He	150 (600)	130 - 150 (520 - 600)	480 - 1000
NF_3	NA	1 - 1.5 (4 - 6)	4 - 20
F_2	0.66 (2.64)	NA	2 - 8
DCl	2.0 (8.0)	2.0 – 2.5 (8 - 10)	16 - 25
HI	0.032 (0.12)	0.04 - 0.07 (0.16 - 0.28)	0.12 - 0.60
HN_3	3.32 (13.3)	3 - 4.5 (12 - 18)	10 - 70
Pressure (Torr)	16	15 - 16	20 - 30

The discharge efficiency was characterized according to the titration methods described previously by Manke and co-workers [28]. Initially, gas-phase titrations were performed by measuring the yield of I atoms with a tunable diode laser (New Focus, Model 6248) that probes the 1.315-μm $I(^2P_{3/2}) - I^*(^2P_{1/2})$, F(3,4) spin-orbit transition. As the difficulty of maintaining high flows of HI increased and the cost of HI became prohibitive, the titration technique was altered by adding HCl as the titrant and monitoring the relative concentration of $HF(v = 0)$ via absorption on nearby HF(2-0) ro-vibrational transitions. To expedite data collection, the diode laser output was split into three beams that probed three streamwise positions along the reactor. Small-signal gain measurements were performed as previously described by Herbelin *et al.* [25].

Since the small-signal gain for AGIL is optimized when the density of $NCl(a^1\Delta)$ is the highest, a series of experiments were performed to determine the optimum conditions for $NCl(a^1\Delta)$ production. This was accomplished by measuring the $NCl(a^1\Delta)$ emission intensity as a function of HN_3 and DCl flow rates for constant NF_3. The $NCl(a^1\Delta)$ emission spectrum was collected with a near-infrared (NIR) Optical Multichannel Analyzer (Roper Scientific, OMA V) attached to a 0.3-m monochromator (Acton Research Corporation). The OMA V consists of a 256-pixel array of InGaAs detectors and a well-resolved $NCl(a^1\Delta)$ spectrum with high signal to noise ratio can be collected in less than 1 s.

Table I compares the typical experimental conditions used in this study to those from AGIL 1. The flow rate values in parentheses in the first and second columns are Herbelin's [25] and Henshaw's [21] values multiplied by four. Since the AGIL 2 device is essentially four times larger than AGIL 1, these were the initial target values for our study. All gas flows were controlled in the same manner as for the previous AGIL 1 studies [21], [25], [28].

III. EXPERIMENTAL RESULTS

A. F Atom Titrations

The initial experiments performed with the AGIL 2 device were gas-phase F + HI titrations [28], where the density of

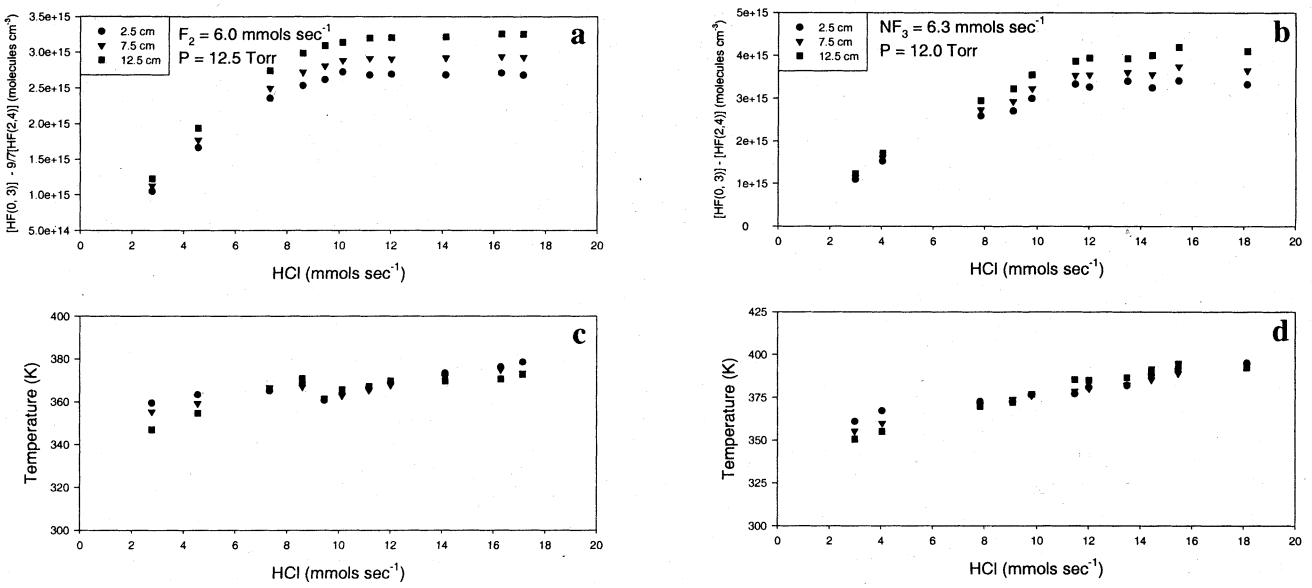

Fig. 2. F + HCl titrations. The upper plot in each panel shows the measured population difference ($[\mathrm{HF}(0,3)] - 9/7[\mathrm{HF}(2,4)]$) as a function of added HCl, see text for details. The lower plot in each panel shows the variation in temperature with added HCl. In all cases, the various symbols indicate different downstream positions: • = 2.5 cm, ▼ = 7.5 cm, and ■ = 12.5 cm downstream from the HI/HN_3 injector blocks.

$I(^2P_{3/2})$ was measured via absorption spectrometry and then related to the density of F atoms produced by the dc discharges via titration plots. Several complications were encountered with this method, all of which could be related to the difficulty of generating and maintaining known, large flows of HI [29]. Gaseous HI is commercially available, but the purity of the bottle contents degrades with time according to the well-known $2HI \leftrightarrow H_2 + I_2$ equilibrium. More seriously, for large flows of HI, liquid and solid particulates may be entrained in the flow that can clog and degrade the performance of the flow-control system. Expansion and cooling of the HI gas after passing through a sonic orifice may lead to condensation along the tubing.

For these reasons, as well as the increasingly prohibitive cost of purchasing large quantities of high purity HI, an alternative titration method was sought and developed. Instead of flowing HI and measuring the yield of atomic I, HCl was added to the flow of F atoms and [HF] was monitored via absorption on a HF(2–0) overtone ro-vibrational transition. Because the F+HCl reaction generates a multitude of HF ro-vibrational states including significant $HF(v = 2)$, the measured absorption signal is proportional to the population difference between HF(0,J) and HF(2,J') and the measured signal does not directly give $[F]_0$. Rather, the yield of F atoms is given by the titration endpoint. As HCl is added to the flow, the absorption signal increases until all of the F atoms are consumed and the initial F atom flow rate is given by the HCl flow necessary to reach the maximum observed signal. Large flow rates of high-purity HCl are easily (and inexpensively) generated because there are no condensation or particulate entrainment issues.

A series of F atom titrations using HCl as the titrant are shown in Fig. 2. The results from these experiments complement the results from the F + HI titrations, and aid in their interpretation [29]. While this method is not as direct or as precise as measuring [I], it is well suited to our application since we do not need a very precise endpoint and are loath to install a complicated system to deliver large flows of pure and particulate-free HI in a reliable manner.

For F_2 and NF_3 = 6 mmol s^{-1} [Fig. 2(a) and (b)], the titration endpoints occur at approximately 11 – 12 mmol s^{-1} of HCl, which in the case of NF_3 corresponds to approximately two atoms per molecule. In the case of F_2, this represents 90%–100% dissociation. The population difference signal increases as the flow progresses downstream, consistent with relaxation of vibrationally excited HF. For F_2, the translational temperature is 360 ± 20 K, while for NF_3, the linewidth analyses give $T = 375 \pm 15$ K. These data are in agreement with the thermocouple data; the NF_3 discharge is slightly hotter than the F_2 discharge. It should be noted that there is considerable uncertainty (at least ±20%) about the titration endpoint because there is not a sharp break between the linear growth and plateau regions of the titration plots and the data is indirectly related to the initial [F]. However, it is clear that a large fraction of molecular F_2 is dissociated and that both F_2 and NF_3 can be used to produce large F atom fluences.

B. Optimization of $NCl(a^1\Delta)$

The energy carrier $NCl(a^1\Delta)$ is produced from F atoms and hydrogen azide by a three-step process described above [reactions (5) – (7)] [20], [22], [23]. According to this mechanism, two F atoms, two DCl molecules, and 1 HN_3 molecule are required to produce a single $NCl(a^1\Delta)$. The stoichiometry can be tested by monitoring the density of $NCl(a^1\Delta)$ via its spontaneous emission signal as a function of added DCl and HN_3.

The conditions for Fig. 3 were $NF_3 = 6$ mmol s^{-1}, $HN_3 = 12$ mmol s^{-1}, and pressure ∼ 12 Torr. A fiber-optic bundle, placed 12.5-cm downstream of the end of the HI/HN_3 injection block was used to collect the emission. Two series of experiments were performed, separated in time by approximately 30 days. For purposes of comparison, the spectral areas are

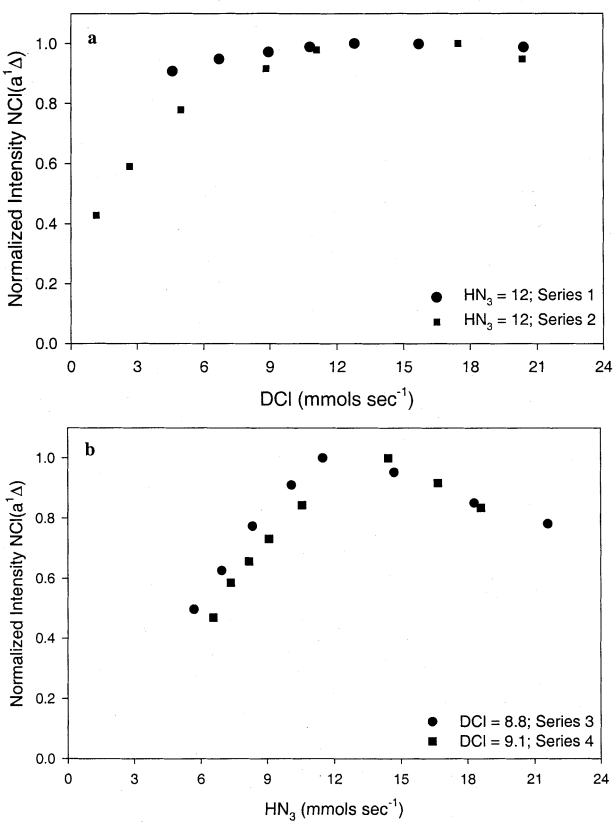

Fig. 3. Optimization of NCl($a^1\Delta$) emission intensity. (a) NCl($a^1\Delta$) versus DCl. The NF_3 flow rate used for these was 6 mmol s^{-1}. The emission intensity of NCl($a^1\Delta$) is optimized at DCl = 12 mmol s^{-1}, consistent with the expectation that NCl($a^1\Delta$) production is optimal when [DCl] = [F] = 2[NF_3], and all of the F atoms have been consumed. (b) NCl($a^1\Delta$) versus HN_3. The NF_3 flow rate used for these experiments was 6 mmol s^{-1}. The emission intensity of NCl($a^1\Delta$) is optimized at HN_3 = 12 mmol s^{-1}. According to the stoichiometry of the F/DCl/HN_3 chemical mechanism for the formation of NCl($a^1\Delta$), the density of NCl($a^1\Delta$) should be optimized at [HN_3] = 0.5[F] = [NF_3] rather than the twofold excess of HN_3 shown here.

normalized to the maximum observed intensity for that experimental series. The two data series are qualitatively the same and the intensity of NCl($a^1\Delta$) reaches a plateau at approximately 12 mmol s^{-1} of DCl. Inasmuch that one would expect the NCl($a^1\Delta$) to optimize at the stoichiometric limit of [DCl] = [F], this supports the F atom titration results which indicate that [F] $\sim$ 2[NF_3]. Furthermore, the intensity of NCl($a^1\Delta$) did not decrease significantly when a nearly twofold excess of DCl was added. The presence of excess DCl does not appear to strongly quench NCl($a^1\Delta$).

In the lower panel of Fig. 3, the flow rates for NF_3 and DCl were held constant (6 and 9 mmol s^{-1}, respectively) while HN_3 was varied from 6 to 24 mmol s^{-1}. For both series of experiments, the maximum yield of NCl($a^1\Delta$) was achieved when $HN_3 \sim 12$ mmol s^{-1}. The Cl/HN_3 stoichiometry suggests that the optimum condition for NCl($a^1\Delta$) production is $HN_3/Cl = 0.5$, and our result $HN_3/Cl \sim 1$ is a factor of two too large. This is not a surprising result considering that Herbelin [25] and Henshaw [21] reported a similar trend for AGIL 1. Their optimum HN_3 : Cl ratios for gain/lasing power were 2.5 and 1.9, respectively.

C. Optimization of $I^*(^2P_{1/2}) - I(^2P_{3/2})$ Small-Signal Gain

Sample results from one series of gain optimization experiments are shown in Fig. 4. In the upper panel, the F_2, DCl, and HI flow rates were fixed at 6, 15, and 0.25 mmol s^{-1}, respectively. At $x = 2.5$ and 7.5 cm, positive gain is observed for a wide range of HN_3 flow rates. For $x = 12.5$ cm, a small absorption signal is observed in all cases. While the dependence of the gain on HN_3 looks similar to the NCl($a^1\Delta$) optimization plot in Fig. 3, the small-signal gain data reaches an optimum at $HN_3 \sim 25$ mmol s^{-1}, approximately a factor of two higher than was required to reach the optimum NCl($a^1\Delta$) intensity. The peak gain for $x = 2.5$ cm and $HN_3 = 20 - 60$ mmol s^{-1} is 2.2×10^{-4} cm^{-1}. The dependence of the small-signal gain on the DCl flow rate is shown in the center panel of Fig. 4. For DCl $\geq$ 12 mmol s^{-1}, the gain is essentially constant at $2.0 \pm 0.2 \times 10^{-4}$ cm^{-1}. This result supports the previous observation that DCl is not a strong quencher of NCl($a^1\Delta$) or $I^*(^2P_{1/2})$ and the F atom titration results which give F = 12 mmol s^{-1} when $F_2 = 6$ mmol s^{-1} is discharged. Finally, in the lower panel, the small-signal gain dependence on the HI flow rate is shown. For $x = 2.5$ cm, the gain is a relatively weak function of HI. For $x = 7.5$ and 12.5 cm, however, the gain decreases dramatically for HI ≥ 0.3 mmol s^{-1}.

Similar plots were generated for a variety of F_2 and NF_3 flow rates. Table II summarizes the optimum gain measured for F_2 =6–8 and NF_3 =4–12 mmol s^{-1}. It is important to note that the results for $NF_3 = 10$ and 12 mmol s^{-1} were not optimized for the HI flow rate. The gain scales more or less monotonically with increasing F atom flow rate when NF_3 is the discharge source of the F atoms. Interestingly, the gain does not appear to scale well when F_2 is discharged even though nearly 100% of the F_2 is dissociated. The highest gain measured in this study was 2.5×10^{-4} cm^{-1}. These results compare favorably with AGIL 1 [21] which gave a maximum gain of 2.7×10^{-4} cm^{-1}. Our peak gain is essentially the same for comparable conditions. However, in contrast to the AGIL 1 results, positive gain does not persist along the length of the reactor.

In the past, we have attributed nonstoichiometric HN_3 : Cl ratios to poor mixing. Visual inspections of the flow did not reveal any obvious mixing problems for either HN_3 or HI. We attempted to test the homogeneity of HN_3 and HI in the flow by measuring the variation of I atom absorption and small-signal gain along the vertical axis of the reactor. The results are shown in the upper and lower panels of Fig. 5. For both plots, the experimental conditions were $F_2 = 8$, HI = 0.4, and DCl = 18 mmol s^{-1}. In the lower panel, $HN_3 = 28$ mmol s^{-1} was added. In the upper panel, the measured ($I(^2P_{3/2})$) is peaked in the center for $x = 2.5$ cm and decreases slightly as the diode probe laser position was shifted away from the centerline of the reactor. The $x = 5$- and 10-cm data are fairly constant across the entire range. Clearly, the injected HI has penetrated into the center of the flow, even at $x = 2.5$ cm. The profile change between $x = 2.5$ cm and $x = 5$ cm, however, suggests that the HI may not be uniformly distributed across the vertical axis at it its injection point, and that some time must elapse before diffusion or another mixing mechanism can establish a homogenous medium. The lower panel data shows that the vertical profile of

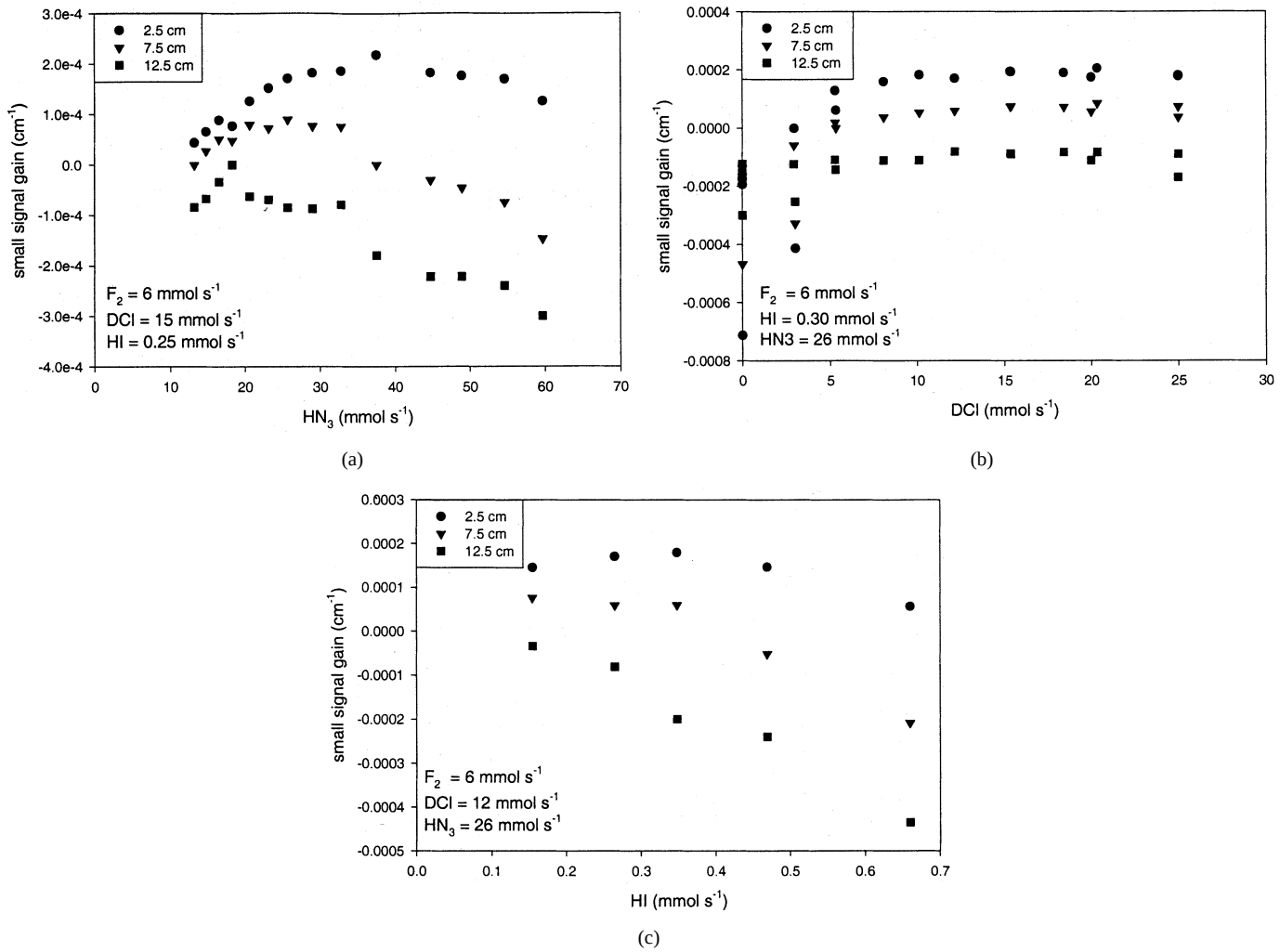

Fig. 4. Optimization of small-signal gain for $F_2 = 6$ mmol s^{-1}. (a) Small-signal gain versus HN_3. The F_2, HI, and DCl flow rates are as indicated in the figure. The highest small-signal gain (2.2×10^{-4} cm^{-1}) is observed for $HN_3 = 38$ mmol s^{-1} and 2.5-cm downstream of the HN_3 injection block. The gain decreases significantly as the flow progresses downstream while smaller variations are observed for increasing or decreasing HN_3 flow rates. (b) Small-signal gain versus DCl. The F_2, HI, and HN_3 flow rates are as indicated in the figure. The highest small-signal gain (2.0×10^{-4} cm^{-1}) is observed for DCl $= 20$ mmol s^{-1} and 2.5-cm downstream of the HN_3 injection block. The gain is relatively constant for DCl $- 12 = 25$ mmol s^{-1} but decreases for DCl < 12 mmol s^{-1}. As noted above, the gain decreases significantly as the flow progresses downstream. (c) Small-signal gain versus HI. The F_2, DCl, and HN_3 flow rates are as indicated in the figure. The highest small-signal gain (1.8×10^{-4} cm^{-1}) is observed for HI $= 0.35$ mmol s^{-1} and 2.5-cm downstream of the HN_3 injection block. The gain decreases significantly as the flow progresses downstream.

TABLE II
SMALL-SIGNAL GAIN SUMMARY

F atom source	Flow rate (mmol s^{-1})	F atom flow rate (mmol s^{-1})	Maximum gain (10^{-4} cm^{-1})
NF_3	4	8	1.04
NF_3	6	12	1.80
NF_3	8	16	2.50
NF_3	10	--[a]	1.81[b]
NF_3	12	--[a]	2.04[b]
F_2	6	10 – 11	2.18
F_2	8	14 – 15	2.05

[a] Titration not performed for this condition.

[b] Gain not optimized for HI flow rate.

the small-signal gain is essentially the same as the ($I(^2P_{3/2})$) data. The addition of 28 mmol s^{-1} of HN_3 (and the accompanying 250 mmol s^{-1} of He) does not appear to affect the degree of penetration or mixing rate of the HI. In fact, the small-signal gain data are consistent with a uniform NCl($a^1\Delta$) density, and efficient mixing of HN_3. We have previously [29] suggested that poor mixing is the dominant factor that limits AGIL performance based on computational fluid dynamics results. Unfortunately, the present results are not conclusive and further tests of the role of mixing will be conducted in the near future.

D. AGIL Power Extraction

Power-extraction experiments for AGIL 2 gave significantly higher powers than AGIL 1. The results are summarized in Table III and Fig. 6. As was the case for AGIL 1, the power-extraction demonstrations required extremely high quality mirrors; the high reflector (HF) and output coupler mirror reflectivities (as measured by cavity ringdown spectroscopy) were 0.9999 and 0.998, respectively. All high reflector optics had a 2-in diameter and a 5-m radius of curvature. The alignment of the resonator was initially accomplished by superimposing a He:Ne laser beam through the centerline of the flow

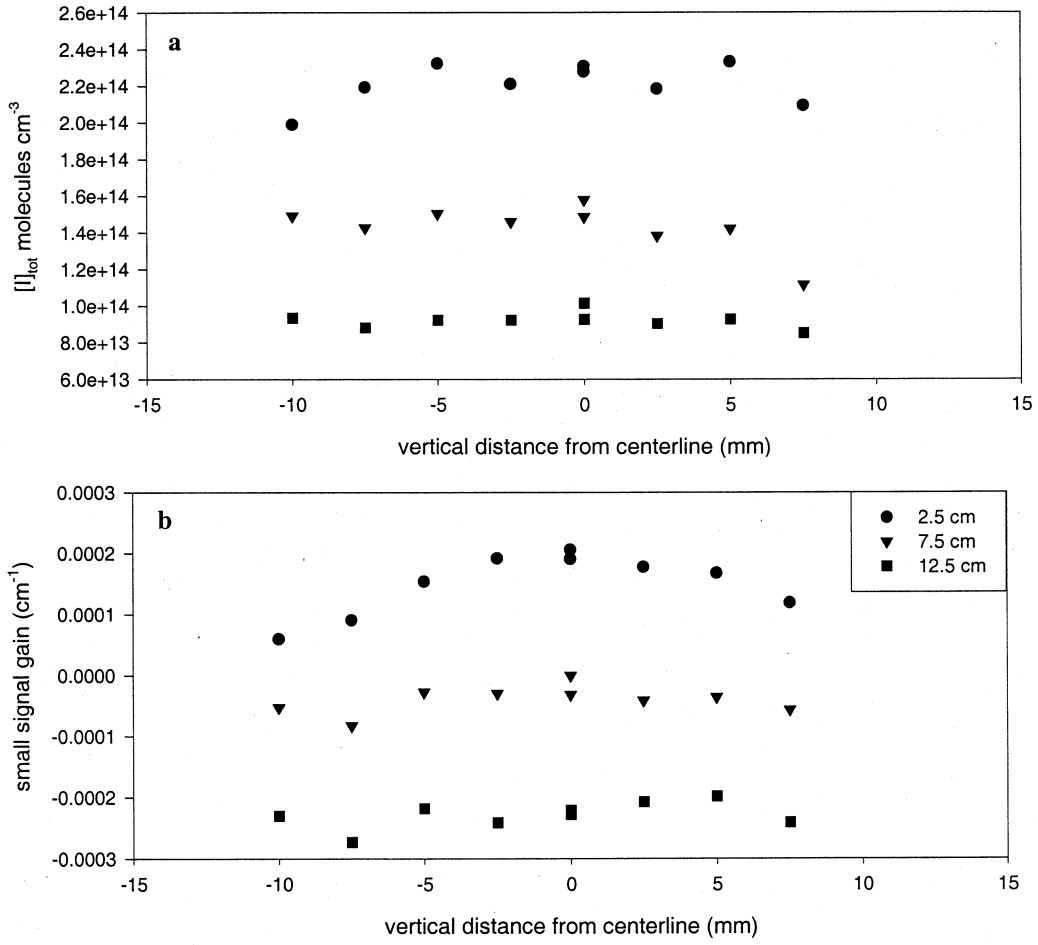

Fig. 5. Vertical profile of small-signal gain and $[I]_{tot}$. (a) Vertical profile of $[I(^2P_{3/2})]$. The experimental conditions were $F_2 = 8$, HI $= 0.4$, and DCl $= 18$ mmol s^{-1}. The density of $I(^2P_{3/2})$ atoms in the absence of HN_3 is shown. The observed profile is slightly peaked. There is a noticeable variation in I atom density along the vertical axis in the absence of HN_3, suggesting that while HI is fully penetrated into the center of the flow, the I atom density is not homogenous across the entire flow profile. (b) Vertical profile of small-signal gain. The experimental conditions were $F_2 = 8$, HI $= 0.4$, DCl $= 18$, and $HN_3 = 28$ mmol s^{-1}. In a pattern similar to the $(I(^2P_{3/2}))$ profile in the upper panel, the small-signal gain is peaked in the center and decreases slightly as the diode probe laser position was shifted. The lack of difference between the upper and lower panels suggests that the injected HN_3 is fully penetrated into the flow and is well mixed.

TABLE III
AGIL 2 POWER-EXTRACTION SUMMARY

Position	Output Coupler Reflectivity	Power (W)
	0.9997[c]	0.5
	0.998[c]	14.3
4.0[a]	0.998[b]	11.6
	0.9973[c]	9.7
	0.9958[d]	6.9

[a] $NF_3 = 8$, DCl $= 25$, $HN_3 = 26$, and HI $= 0.5$ mmol s^{-1}.

[b] Concave with 5-m radius of curvature.

[c] Flat mirror.

[d] Concave with 2-m radius of curvature.

reactor and then adjusting the resonator mirrors such that the reflected beams from the resonator mirrors were collinear with the reactor centerline. It was subsequently learned that much more reliable and reproducible alignments could be achieved with an auto-collimating alignment telescope.

Fig. 6 shows the relationship between out-coupled power versus HI flow rate for two different downstream positions, $x = 1.5$ and 4.0 cm. For the sake of convenience, the HN_3 and DCl flow rates were fixed at the previously determined optimum values, 26 and 25 mmol s^{-1}, respectively. In the upper panel, series A and B were measured using a resonator aligned with the He:Ne laser. Series C and D were measured after alignment with the alignment telescope. Clearly, the latter method gave higher powers, most likely due to an improved alignment. Interestingly, the extracted power was higher at $x = 1.5$ cm for NF_3 as the discharge source of F atoms. At the next downstream position, NF_3 and F_2 give comparable power values. We attribute this difference to the fact that the F_2 discharge gives slightly lower temperatures than NF_3. Since the rate determining step for $NCl(a^1\Delta)$ generation [reaction (6)] is strongly temperature dependent, it is sensible that the hotter, NF_3 case would reach the peak $NCl(a^1\Delta)$ density at an earlier position (i.e., earlier time) in the reactor. All attempts to measure power at $x = 6.5$ cm downstream were unsuccessful, even with a low threshold cavity (i.e., $OC = 99.97\%$ reflectivity). This result is consistent with the small-signal gain measurements that gave very low or no gain at $x = 7.5$ cm (see Figs. 4 and 5). Clearly, the gain is strongly dependent on

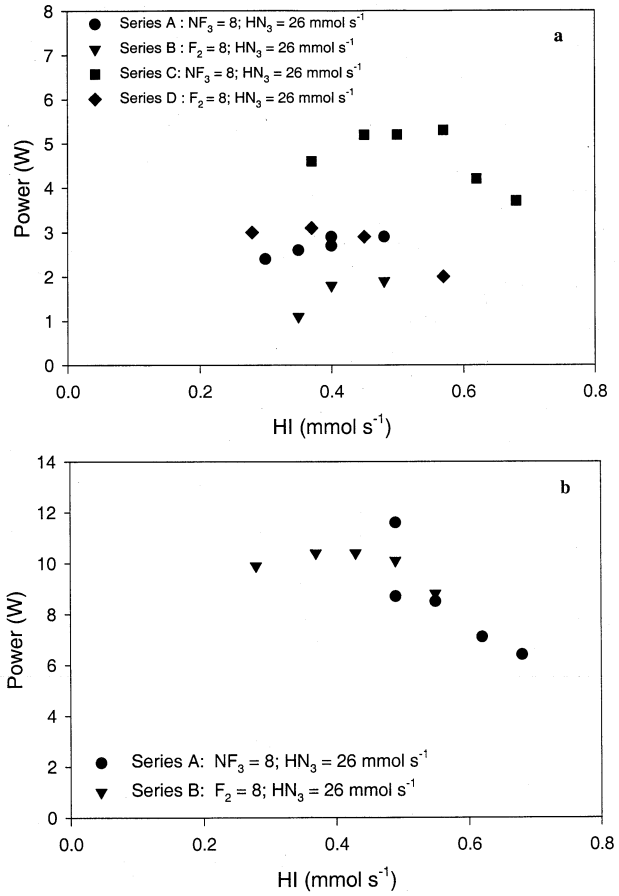

Fig. 6. AGIL power extraction versus HI. (a) Power extraction versus HI for $x = 1.5$ cm downstream of the HI/HN_3 injection block. Series A and B were collected on the same day, using a He:Ne laser to optimize the alignment. Series C and D were measured on a different day and an auto-collimating alignment telescope was used to optimize the alignment. The resonator consisted of two 2" concave (5-m radius of curvature) mirrors with measured reflectivities of 0.9999 and 0.998. (b) Power extraction versus HI for $x = 4.0$ downstream of the HI/HN_3 injection block. Series A and B were collected with the resonator centered 4.0-cm downstream of the end of the HI/HN_3 injection block. The reagent flow conditions are as indicated in the figure.

the reaction time. A full explanation of this behavior requires additional analysis by computational fluid dynamics.

Table III summarizes the effect of varying the output coupler reflectivity for $x = 4.0$ cm, and constant reagent flow rates of $NF_3 = 8$, $HN_3 = 26$, DCl = 25, and HI = 0.5 mmol s^{-1}. The mirror reflectivities for the various outcouplers were estimated from total transmission measurements and assuming $R = 1.0 - T$. The power versus reflectance data can be used to confirm the directly measured small-signal gain values. The x-intercept of a $1 - R_2$ versus power plot gives the mirror reflectivity (R_2) value for the threshold condition

$$g_0 = g_{\text{th}} = \frac{-\ln(R_1 R_2)}{2L}. \tag{8}$$

A crude extrapolation of the data in Table III gives $R_2 \sim 0.993$. For $R_1 = 0.9999$ and $L = 20$ cm the estimated threshold gain, 1.8×10^{-4} cm^{-1}, is in good agreement with the directly measured value ($2.0 - 2.5 \times 10^{-4}$ cm^{-1}). The $x = 4.0$ cm data suggests that even higher outcoupled power may be possible for $0.9999 < R_2 < 0.998$. Further enhancements to the extracted power may be realized by changing the mirror size (x_c), moving the mirror position (x), or increasing the F atom flow rate.

IV. Disscussion and Conclusions

The fundamental performance characteristics of AGIL 2 have been examined. F + HI and F + HCl titrations have been used to determine the F atom production efficiency of the dc discharges. Optimum conditions for the production of NCl($a^1\Delta$) and $I(^2P_{1/2}) - I(^2P_{3/2})$ gain have been identified for a moderate range of reactor conditions. To date, the highest observed small-signal gain for AGIL 2 is 2.5×10^{-4} cm^{-1}, essentially equivalent to the highest gain measured in AGIL 1. The highest observed power was 15 W.

The most critical experiments that directly address the scalability of AGIL remain to be completed. In particular, it has yet to be shown conclusively that [NCl($a^1\Delta$)] and gain scale with increasing [Cl]. The AGIL 1 and AGIL 2 data strongly suggest that increases in [NF_3] (which leads to higher [F] and thus, higher [Cl]) leads to higher gain and higher extracted power. However, the range of NF_3 and F_2 flow rates tested by AGIL 1 and AGIL 2 is rather limited. Significantly higher F and Cl atom flow rates can be generated by chemical combustors or high power microwave devices [30]. An AGIL device employing these technologies is currently in the planning and design stages.

Acknowledgment

The authors wish to acknowledge helpful discussions with Profs. M. C. Heaven (Emory University) and R. D. Coombe (Denver University) regarding AGIL chemistry.

References

[1] W. E. McDermott, N. R. Pchelkin, D. J. Benard, and R. R. Bousek, "An electronic transition chemical laser," *Appl. Phys. Lett*, vol. 32, pp. 469–470, 1978.
[2] M. C. Heaven, "Chemical dynamics in chemical laser media," in *Chemical Dynamics in Extreme Environments, Advanced Series in Physical Chemistry*, R. A. Dressler, Ed. Singapore: World Scientific, 2001.
[3] A. C. Becker and U. Schurath, "Matrix-isolated NCl: Radiative rates for $b^1\Sigma^+ - a^1\Delta$;$b^1\Sigma^+ - X^3\Sigma^-$ and $a^1\Delta - X^3\Sigma^-$ in solid argon," *Chem. Phys. Lett.*, vol. 160, pp. 586–590, 1989.
[4] D. R. Yarkony, "On the radiative lifetimes of the $b^1\Sigma^+$ and $a^1\Delta$ states in NCl," *J. Chem. Phys.*, vol. 86, pp. 1642–1643, 1987.
[5] M. Bettendorff and S. D. Peyerimhoff, "Electronic-structure of the radicals-NF and NCl 1. Potential-energy curves for NF," *Chem. Phys.*, vol. 99, pp. 55–72, 1985.
[6] K. B. Hewett, G. C. Manke II, D. W. Setser, and G. Brewood, "Quenching rate constants of NCl($a^1\Delta$) at room temperature," *J. Phys. Chem. A.*, vol. 104, pp. 539–551, 2000.
[7] K. Y. Du and D. W. Setser, "Quenching rate constants of NF($a^1\Delta$) at room-temperature," *J. Phys. Chem.*, vol. 94, pp. 2425–2435, 1990.
[8] J. M. Herbelin and R. A. Klingberg, *Int. J. Chem. Kinet.*, vol. 16, p. 849, 1984.
[9] G. A. Capelle, D. G. Dutton, and J. I. Steinfeld, *J. Chem. Phys.*, vol. 69, p. 5140, 1978.
[10] D. J. Benard, *J. Appl. Phys.*, vol. 74, p. 2900, 1993.
[11] D. J. Benard and B. K. Winker, *J. Appl. Phys.*, vol. 69, p. 2805, 1991.
[12] D. J. Benard, B. K. Winker, T. A. Seder, and R. H. Cohn, *J. Phys. Chem.*, vol. 93, p. 4790, 1989.
[13] D. J. Benard, E. Boehmer, H. H. Michels, and J. J. A. Montgomery, *J. Phys. Chem.*, vol. 98, p. 8952, 1994.
[14] E. Boehmer and D. J. Benard, *J. Phys. Chem.*, vol. 99, p. 1969, 1995.
[15] D. J. Benard and E. Boehmer, *Appl. Phys. Lett.*, vol. 65, p. 1340, 1994.
[16] D. J. Benard, *J. Phys. Chem.*, vol. 100, p. 8316, 1996.

[17] K. Y. Du and D. W. Setser, "Quenching reactions of NF($a^1\Delta$) by Cl_2 ; ClF ; Br_2 ; ICl ; IF ; and I_2," *J. Phys. Chem.*, vol. 96, pp. 2553–2561, 1992.

[18] H. Cha and D. W. Setser, "NF($b^1\Sigma^+$) quenching rate constants by halogens and interhalogens and the excitation rate-constant for IF(B) formation," *J. Phys. Chem.*, vol. 91, pp. 3758–3767, 1987.

[19] A. J. Ray and R. D. Coombe, "Energy-transfer from NCl($a^1\Delta$) to iodine atoms," *J. Phys. Chem.*, vol. 97, pp. 3475–3479, 1993.

[20] T. L. Henshaw, S. D. Herrera, and L. A. V. Schlie, "Temperature-dependence of the NCl($a^1\Delta$) + I($^2P_{3/2}$) reaction from 300 to 482 K," *J. Phys. Chem. A*, vol. 102, pp. 6239–6246, 1998.

[21] T. L. Henshaw, G. C. Manke II, T. J. Madden, M. R. Berman, and G. D. Hager, "A new energy transfer chemical laser at 1.315 μm," *Chem. Phys. Lett.*, vol. 325, pp. 537–544, 2000.

[22] G. C. Manke II and D. W. Setser, "Kinetics of NCl($a^1\Delta$ and $b^1\Sigma^+$) generation: The Cl+N_3 rate constant, the NCl($a^1\Delta$) product branching fraction , and quenching of NCl($a^1\Delta$) by F and Cl atoms," *J. Phys. Chem. A*, vol. 102, pp. 7257–7266, 1998.

[23] ——, "Measuring gas-phase chlorine atom concentrations: Rate constants for Cl + HN_3 ; CF_3I ; and C_2F_5I," *J. Phys. Chem. A*, vol. 102, pp. 153–159, 1998.

[24] G. C. Manke II, T. L. Henshaw, T. J. Madden, and G. D. Hager, "Temperature dependence of the Cl + HN_3 reaction from 300 to 480 K," *Chem. Phys. Lett.*, vol. 310, pp. 111–120, 1999.

[25] J. M. Herbelin, T. L. Henshaw, B. D. Rafferty, B. T. Anderson, R. F. Tate, T. J. Madden, G. C. Manke, and G. D. Hager, "The measurement of gain on the 1.315 μm transition of atomic iodine in a subsonic flow of chemically generated NCl($a^1\Delta$)," *Chem. Phys. Lett.*, vol. 299, pp. 583–588, 1999.

[26] R. D. Bower and T. T. Yang, "I($^2P_{1/2}$) produced by the energy-transfer from NCl($a^1\Delta$) to I($^2P_{3/2}$)," *J. Opt. Soc. Amer. B*, vol. 8, pp. 1583–1587, 1991.

[27] A. J. Ray and R. D. Coombe, "An I^* laser-pumped by NCl($a^1\Delta$)," *J. Phys. Chem.*, vol. 99, pp. 7849–7852, 1995.

[28] G. C. Manke II, T. L. Henshaw, T. J. Madden, J. M. Herbelin, B. D. Rafferty, and G. D. Hager, "Characterizing fluorine and chlorine atom flow rates using iodine atom spectrometry," *AIAA J.*, vol. 39, pp. 447–454, 2001.

[29] G. C. Manke II, T. L. Henshaw, C. B. Cooper, and G. D. Hager, "Recent progress in the development of a multi-watt all gas-phase iodine laser (AGIL)," presented at the 33rd AIAA Plasmadynamics and Lasers Conf., Maui, HI, 2002.

[30] S. J. Davis, D. B. Oakes, M. E. Read, and A. H. Gelb, "Atomic fluorine source for chemical lasers," in *Proc. SPIE, Gas and Chemical Lasers and Intense Beam Applications III*, San Jose, CA, 2002.

Gerald C. Manke, II received the B.A. degree in chemistry from Wartburg College, Waverly, IA, in 1992 and the Ph.D. degree in physical chemistry from Kansas State University, Manhattan, in 1997.

He is a Research Chemist in the Directed Energy Directorate (Gas and Chemical Lasers Branch) of the Air Force Research Laboratory, Kirtland AFB, NM. He is the principal investigator and co-inventor for the all gas-phase iodine laser (AGIL).

Chris Cooper received the B.S. degree in chemical engineering (*cum laude*) from the University of New Mexico, Albuquerque, in 1997.

He is a Chemical Engineer with Boeing-Rocketdyne, Kirtland AFB, NM. He is the Project Engineer for the all gas-phase iodine laser and has worked as a contractor for the Air Force Research Lab for almost three years.

Mr. Cooper received the Reibosomer Award for Excellence in Chemistry in 1993.

Shiv C. Dass received the M.S. degree in physics and the Ph.D. degree from University of New Brunswick.

He is a Senior Scientist with Boeing-Rocketdyne, Kirtland AFB, NM, where he works in the high-energy laser research area of the Air Force Research Laboratory. He has been working in the field of lasers and laser electrooptical systems for the past 25 years. He previously worked in a number of laser manufacturing industries in North America. He has published more than 15 research papers in scientific journals and holds one U.S. and international patent.

Timothy J. Madden, photograph and biography not available at the time of publication.

Gordon D. Hager received the Ph.D. degree in chemical physics from Washington State University, Pullman, in 1973.

He has been a Research Scientist with the U.S. Air Force Research Laboratory, Kirtland AFB, NM, since 1982. His area of expertise is high-power gas phase and chemical lasers.